Sensors & Actuators: B. Chemical 418 (2024) 136226

Contents lists available at ScienceDirect

Sensors and Actuators: B. Chemical

journal homepage: www.elsevier.com/locate/snb

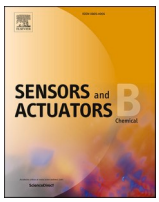

A dual-channel sensing platform for ATP and copper ions via the target-induced peroxidase mimics activity and fluorescence variations of iron oxide nanoparticles-modified metal-organic frameworks

Yani Liu [a,b], Haoyu Chen [a], Lin Chai [a], Jing Liu [a], Shu Huang [b,*], Feng Liu [a], Mingjie Wei [c], Xiaohua Zhu [a], Youyu Zhang [a], Meiling Liu [a,*], Shouzhuo Yao [a]

[a] Key Laboratory of Chemical Biology & Traditional Chinese Medicine Research (Ministry of Education, China), College of Chemistry and Chemical Engineering, Hunan Normal University, Changsha 410081, China
[b] Department of Orthopedics, Hunan Provincial People's Hospital, The First-Affiliated Hospital of Hunan Normal University, Changsha 410005, China
[c] School of Pharmacy, Xianning Medical College, Hubei University of Science and Technology, Xianning 437100, China

ARTICLE INFO

Keywords:
PCN-224@Fe_2O_3
Peroxidase-like activity
ATP
Copper ions
Colorimetric-fluorescence dual-channel sensing

ABSTRACT

The simultaneous or continuous detection of multiple targets in complex samples is for various applications, notably in medical diagnostics and environmental monitoring. A novel dual-channel colorimetric and fluorescent method has been developed for the continuous detection of adenosine triphosphate (ATP) and copper ions based on PCN-224@Fe_2O_3, which exhibits both fluorescent and enhanced peroxidase-like (POD-like) properties. The synthesis of PCN-224@Fe_2O_3 involved the in-situ growth of ferric oxide on Zr-based metal-organic frameworks (PCN-224). Through catalyzing the colorless compound 3,3′,5,5′-tetramethylbenzidine (TMB) to produce a blue product (oxTMB) in the presence of H_2O_2, PCN-224@Fe_2O_3 allows for the detection of ATP and copper ions. The unique mechanism involves ATP weakening the POD-like activity of PCN-224@Fe_2O_3 by forming Zr-O-P bonds with Zr in PCN-224, which also leads to fluorescence recovery. Copper ions, through chelating with ATP, counteract the effect of ATP on PCN-224@Fe_2O_3, resulting in increased POD-like activity and the amount of oxTMB alongside the quenching of the fluorescence of the system. This facilitates colorimetric "on-off-on" and fluorescence "off-on-off" switch sensing for ATP and Cu^{2+}. The application of PCN-224@Fe_2O_3 in the detection of ATP and Cu^{2+} in human serum yielded satisfactory results. This innovative approach not only provides a means to regulate the mimic activity of oxides but also presents a convenient, sensitive, and accurate detection method for ATP and Cu^{2+}, significantly broadening the potential application of MOFs and nanozymes in bioanalysis.

1. Introduction

Accurate detection and differentiation of small molecules in complex samples play a vital role in medical diagnostics and environmental monitoring. Sensors possess qualities such as stability, high selectivity, applicability to complex sample matrices, and quick response to target variations [1]. Additionally, the capability to detect multiple targets simultaneously or continuously can offer more comprehensive insights and enhance sensor effectiveness [2]. It's important to note that while Cu^{2+} is necessary for some biological functions, an excess accumulation in the body can lead to health issues like liver toxicity, neurodegenerative diseases, and Wilson's disease due to its interference with enzyme reactions and disruption of energy metabolism. The presence of excess free Cu^{2+} ions has the potential to instigate the formation of free radicals, instigating oxidative damage and genetic alterations [3]. Adenosine triphosphate (ATP), a critical nucleoside triphosphate that facilitates energy supply in biological systems, holds a fundamental role in cellular processes. Imbalance in ATP hydrolysis can alter the rate and concentration of ATP burning, thereby triggering a series of diseases, including hypoglycemia, ischemia, hypoxia, and Parkinson's disease [4]. Therefore, monitoring of Cu^{2+} and ATP levels in real-time is imperative for unraveling their physiological functions and diagnosing associated diseases [5]. Consequently, the development of sensing platforms for detecting Cu^{2+} and ATP levels in blood or cells emerges as

* Corresponding authors.
E-mail addresses: huangshu@hunnu.edu.cn (S. Huang), liumeilingww@126.com, liuml@hunnu.edu.cn (M. Liu).

https://doi.org/10.1016/j.snb.2024.136226
Received 17 April 2024; Received in revised form 19 June 2024; Accepted 30 June 2024
Available online 14 July 2024

a worthwhile endeavor [6].

Dual-mode sensing technology offers many advantages in analytical processes, allowing for efficient and flexible applications in different detection environments [7]. By validating signals from both modes, it ensures the accuracy and reliability of detection results [8]. Fluorescence/colorimetric dual-mode sensors have attracted more attention due to their ability to simultaneously provide highly sensitive signals, along with advantages such as low cost, ease of use, and portability [9]. There is a lack of reports on chemical sensors capable of continuously detecting ATP and Cu^{2+} using both fluorescence and colorimetric methods, making them a particularly attractive area for further research and development.

Nanozymes offer several advantages over natural enzymes, such as low cost, good stability, and simple preparation processes [10], which have gradually replaced natural enzymes in various fields such as biocatalysis, biosensing, and cancer treatment, and show significant potential in food analysis and disease diagnosis. Many nanomaterials exhibit excellent enzyme-like activity and good stability, such as metal oxides and noble metal nanoparticles (NPs) [11]. Iron oxide NPs and their composites inherently exhibit peroxidase-like (POD-like) activity toward common chromogenic substances, enabling the development of high-performance biosensors for the detection of various biomolecules. However, these materials often require relatively high temperatures (40–45 °C) for optimal activity, limiting the sensitivity of the application for detecting disease-specific biomolecules at room temperature [12]. Strategies such as functionalization [13], atomic doping [14], and decoration on other nanomaterials [15] can enhance the activities and affinities to the substrates. For instance, modifying ssDNA on CoOOH nanosheets through electrostatic attraction and π-π stacking interactions enhances the nanozyme activity of CoOOH. In addition, loading of copper oxide nanoparticles onto polyoxometalate nanomaterials has been shown to enhance the multiple enzyme-like activities of copper oxide. Therefore, regulating the microenvironment of oxide nanoparticles may be an effective strategy to further enhance their POD-like activity.

Metal-organic frameworks (MOFs) stand out as highly promising materials due to their tailored structure and tunable properties achieved through the periodic bonding of organic ligands to inorganic metal clusters [16]. Various MOFs such as Fe-MOF, Zr-MOF, Cu-MOF find extensive utility in environmental applications, facilitating pollutant detection serving as adsorbents or photocatalysts. Porphyrins and their derivatives exhibit remarkable visible light response and significant Stokes shift, offering low background signal and exceptional anti-interference capabilities. In particular, PCN-224, a stable MOF synthesized from zirconium oxide clusters and porphyrin ligands, not only possesses general properties of other MOFs but also has impressive tunable fluorescence properties [17]. Using the PCN-224 as a support, Pt NP_S can be loaded, thereby enhancing the enzyme-like activity of Pt NP_S and aiding in the mass transfer of TMB, H_2O_2, and their reaction intermediates [18]. Ren et. al designed a multifunctional "three-in-one" Zr-MOF, named PP-HRP-iDNA, which serves as a dual-signal readout biosensing platform with fluorescence and colorimetric, demonstrating high sensitivity in the detection of aflatoxin B1 and Salmonella enterica [19]. The use of PCN-224 as a fluorescent signal probe not only enhances the nanozyme activity for colorimetric analysis but can utilize its fluorescent properties to construct a fluorescence/colorimetric dual-channel sensing platform. To date, there are no reports on the continuous detection of ATP and copper ions using a dual-mode detection strategy involving Fe_2O_3 nanoparticles and PCN-224.

In this study, as shown in Scheme 1, PCN-224 was synthesized using TCPP and zirconium oxide clusters as precursors, which served as support for loading Fe_2O_3 NPs. A two-channel detection platform was established, combining colorimetric and fluorescence tailored for specific detection of ATP and Cu^{2+}. The resulting PCN-224@Fe_2O_3 composite exhibited significantly enhanced POD-like activity, which was attributed to the increased local concentration of Fe_2O_3 NPs and iron active sites on the unique structure of PCN-224. In the presence of ATP, the catalytic activity of the PCN-224@Fe_2O_3 towards TMB oxidation

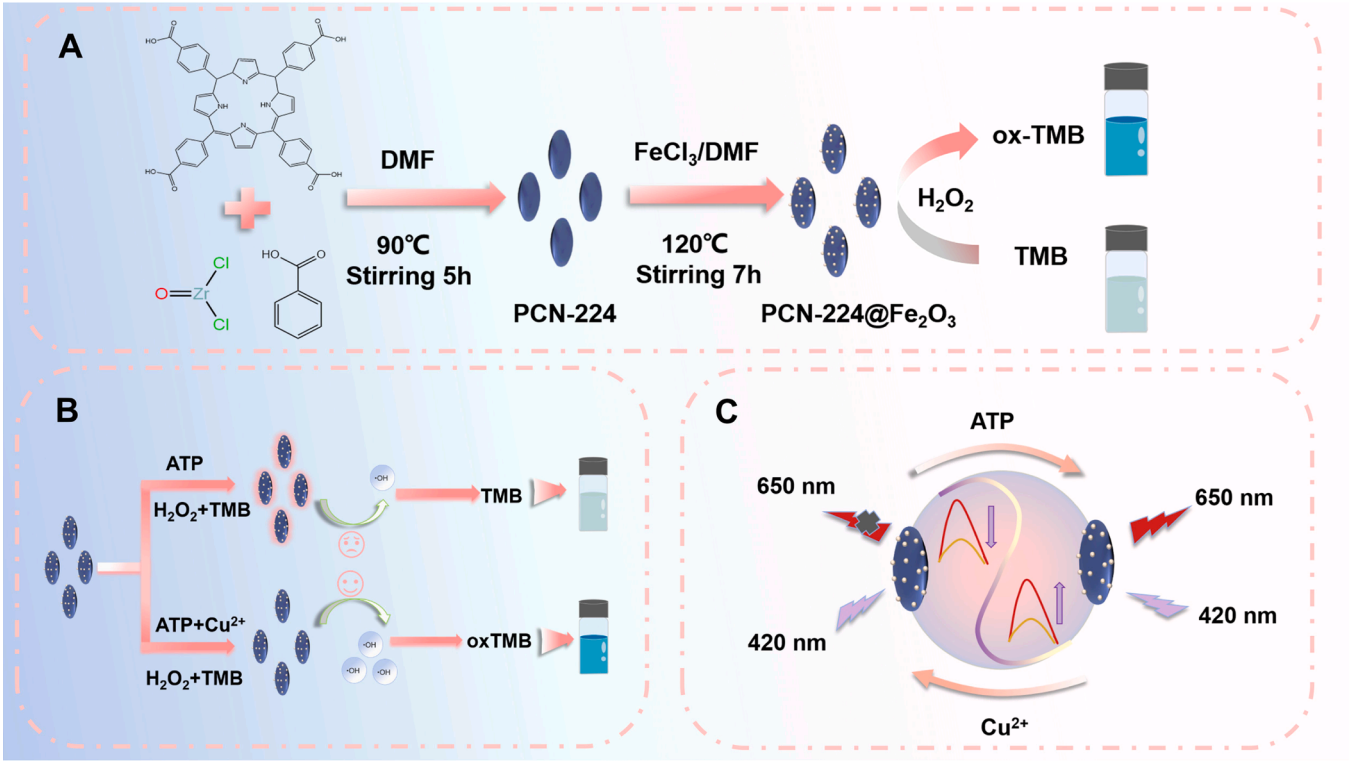

Scheme 1. Schematic illustration of (A) the synthesis process of PCN-224@Fe_2O_3. (B-C) Construction of the dual-mode sensing platform for ATP and Cu^{2+} using colorimetric (B) and fluorescence methods (C) based on PCN-224@Fe_2O_3.

decreased, while the fluorescence in the system recovered. Upon the introduction of Cu^{2+}, the POD-like properties were restored, accompanied by fluorescence quenching. The detection mechanism was carefully analyzed and revealed the formation of Zr-O-P bonds between ATP and PCN-224@Fe_2O_3, leading to ATP attached on the surface of PCN-224@Fe_2O_3 and reduced the exposure of Fe active sites. The alteration of the structure of PCN-224@Fe_2O_3 at a certain concentration of ATP leads to the release of TCPP with red fluorescence. Addition of Cu^{2+} facilitated complexation with ATP, allowing Cu^{2+} to interact with TCPP or PCN-224 and quench the fluorescence of the system. This sensor provides fluorescence/colorimetric dual-mode detection of ATP and Cu^{2+}, increasing sensitivity and minimizing false positive and negative results. This study not only presents a novel strategy for enhancing nanozyme activity but also holds promise for continuous detection by tuning the nanozyme mimetic properties for various biosensing applications, underscoring its significant scientific value.

2. Experimental section

2.1. Reagents and instruments

Zirconium oxychloride octahydrate ($ZrOCl_2{\cdot}8\,H_2O$, AR), 3,3′,5,5′-tetramethylbenzidine (TMB), glutathione (GSH, AR), adenosine triphosphate (ATP) were provided by Shanghai Maclin Biochemical Technology Co., Ltd. Benzoic acid (BA, AR), ascorbic acid (AA, AR), anhydrous sodium acetate (AR), sodium chloride (AR), calcium chloride dihydrate (AR), magnesium acetate tetrahydrate (AR), copper nitrate ($Cu(NO_3)_2$, AR), anhydrous ferric chloride ($FeCl_3$), N,N-dimethylformamide (DMF), dimethyl sulfoxide (DMSO), acetic acid, were provided by Hu'shi. Phthalic acid (TA, 98 %), hydrochloric acid was provided by China National Pharmaceutical Group Chemical Reagent Co., Ltd. Lead chloride (AR), dopamine (DA), Tetra(4-carboxyphenyl) porphyrin (TCPP), Fe(III)meso-Tetra(4-carboxyphenyl) porphyrin Chloride were purchased from Shanghai Aladdin Reagent Co., Ltd. D-cysteine (AR) was provided by Xiyashiji. Tris ($C_4H_{11}NO_3$, AR) was provided by Beijing Bobo Toda Technology Co., Ltd. Iron chloride (AR), manganese chloride (AR) were provided by Tianjin Fengchuan Chemical Reagent Technology Co., Ltd. Hydrogen peroxide (H_2O_2) was provided by China Xilong Science Co., Ltd. All solutions were prepared using ultrapure water.

Ultraviolet spectra were obtained on UV-2600i spectrophotometer (Shimadzu, Japan). Fourier transform infrared (FTIR) spectra were obtained on Nexus-870 (Thermo Scientific, America). Fluorescence spectra were recorded on a fluorescence spectrophotometer (F-7000, Hitachi, Japan). Zeta potential data were recorded on ZS 90. X-ray diffraction (XRD) spectra and X-ray photoelectron spectroscopy (XPS) data were obtained using Rigaku 2500 X-ray diffractometer (Thermo Scientific Ka, UK). Transmission electron microscopy (TEM) and high-resolution transmission electron microscopy (HRTEM) images as well as EDX and mapping images were obtained using Tecnai G2F20 (FEI, USA). High resolution mass spectrometry (HR-MS) was obtained by Thermo Scientific Qex Active Orbit Rap (USA).

2.2. Synthesis of PCN-224@Fe_2O_3

PCN-224 was synthesized according to literature with slight modification [20]: A mixture of 150 mg $ZrOCl_2{\cdot}\,8\,H_2O$, 50 mg TCPP, and 1400 mg benzoic acid was dissolved in 50 mL DMF under sonication, thoroughly mixed, and then transferred to a round-bottom flask for a 5 h reaction at 90 ℃. After cooling to room temperature, the reaction mixture was washed thrice with DMF, and the resulting product was dried at 60 ℃ overnight.

To prepare PCN-224@Fe_2O_3, 30 mg of the synthesized PCN-224 was combined with 40 mg of anhydrous iron chloride, dissolved in 10 mL DMF, sonicated until complete dissolution, stirred at room temperature for 10 min, and then subjected to a 7 h reaction in a 120 ℃ oil bath. After cooling, the mixture was washed thrice with DMF, and the final product was dried at 60 ℃ overnight. To further obtain better performance of the sensor, the ratio of Fe_2O_3 NPs to PCN-224 was optimized. To prepare PCN-224@Fe_2O_3 with different ratios, 10 mg, 30 mg and 50 mg of PCN-224 were combined with 40 mg of $FeCl_3$, and the procedures were similar to above, which obtained the products of PCN-224–10@Fe_2O_3, PCN-224–30@Fe_2O_3, PCN-224–50@Fe_2O_3. For comparison, Fe_2O_3 NPs were synthesized by dissolving 40 mg $FeCl_3$ in 10 mL DMF, subjecting the solution to sonication, stirring at room temperature for ten minutes, and then reacting in a 120 ℃ oil bath for 7 hours.

2.3. POD-like activity and kinetics study of Fe_2O_3 NPs and PCN-224@Fe_2O_3

The kinetic assay was investigated by keeping the concentration of one substrate (TMB or H_2O_2) constant and varying another to monitor the absorbance change of ox-TMB at 652 nm. Keeping the concentration of PCN-224@Fe_2O_3 or Fe_2O_3 NPs constant at 50 $\mu g{\cdot}mL^{-1}$, different concentrations of H_2O_2 or TMB were added in HAc-NaAc (pH 4.5) with fixed total volume of 1 mL, reacted at 35 ℃ for 30 min, and the UV spectra were measured and the absorbance at 652 nm ($A_{652\,nm}$) were recorded to obtain the Michaelis-Menten equation for H_2O_2 and TMB. The kinetic parameters were calculated from the Michaelis-Menten equation:

$$1/V = K_m/V_{max} \times 1/[S] + 1/V_{max} \quad (1)$$

Where V, K_m, V_{max}, [S] represent the reaction initial velocity, Michaelis constant, maximal reaction velocity, and the concentration of the substrate, respectively.

2.4. Detection of ATP and copper ions based on the POD-like activity of PCN-224@Fe_2O_3

Different concentrations of ATP were added to a mixture containing 100 μL PCN-224@Fe_2O_3 (50 $\mu g{\cdot}mL^{-1}$), 100 μL H_2O_2 (10 mM), 50 μL TMB (0.4 mM), and 700 μL HAc-NaAc (pH 4.5). The final volume was adjusted to 1 mL before the reaction at 35 ℃ for 30 min. UV spectra were measured and $A_{652\,nm}$ was recorded.

The detection for Cu^{2+} was as follows: different concentrations of copper ions were added to a solution containing 100 μL PCN-224@Fe_2O_3 (50 $\mu g{\cdot}mL^{-1}$), 100 μL H_2O_2 (10 mM), 50 μL TMB (0.1 mM), 50 μL ATP (50 μM), 600 μL HAc-NaAc (pH 4.5). The final volume was controlled at 1 mL, and the reaction was conducted at 35 ℃ for 30 minutes. UV spectra were measured and $A_{652\,nm}$ was recorded.

2.5. Detection of ATP and copper ions based on fluorescence of PCN-224@Fe_2O_3

Different concentrations of ATP to the solution containing 100 μL PCN-224@Fe_2O_3 (50 $\mu g{\cdot}mL^{-1}$) and 800 μL Tris-HCl (pH 7.5). The final volume was controlled to 1 mL, and the reaction was conducted at 50 ℃ for 50 minutes, followed by fluorescence spectra measurement.

For the detection of Cu^{2+}, different concentrations of Cu^{2+} were added to the solution containing 100 μL PCN-224@Fe_2O_3 (50 $\mu g{\cdot}mL^{-1}$), 100 μL ATP (50 μM), and 700 μL Tris-HCl (pH 7.5). The final volume was controlled at 1 mL. After reaction at 50 ℃ for 60 minutes, the fluorescence spectra were monitored.

2.6. Real sample analysis

Human serum samples were obtained from the Affiliated Hospital of Hunan Normal University and were handled in compliance with the Guidelines for Care and Use of Laboratory Animals, approved by the Biomedical Research Ethics Committee of Hunan Normal University. Initially, the sample was subjected to acid precipitation at 12000 rpm

for 15 minutes to remove fibrous protein precipitates, pH neutralization, followed by oxidation process in air for 2 hours to remove interfering substances. Diluted serum was then prepared for analysis. Tap water, obtained from the School of Chemistry and Chemical Engineering of Hunan Normal University, underwent a similar centrifugation process to remove impurities prior to dilution. The proposed sensing platform was utilized to detect ATP and Cu^{2+} in human serum samples using standard addition method to validate the efficacy of the method.

3. Result and discussion

3.1. Characterization of PCN-224@Fe_2O_3

Transmission electron microscopy (TEM) and energy-dispersive X-ray spectroscopy (EDS) were used to analyze the morphology and elemental composition of the nanocomposite. The PCN-224@Fe_2O_3 exhibits a shuttle-shaped structure [20], with Fe_2O_3 nanoparticles uniformly distributed on its surface, as shown in Fig. 1 A. The high-resolution transmission electron microscopy (HRTEM) in Fig. 1B shows a lattice spacing of 0.265, which is the characteristic of the (104) plane of cubic phase of Fe_2O_3 [21]. The EDX image in Fig. 1 C displays peaks corresponding to C, H, O, N, Zr, and Fe elements in PCN-224@Fe_2O_3, confirming the successful loading of Fe_2O_3 NPs onto PCN-224. The narrow sharp peaks at 2θ values of 24.1°, 33.2°, 35.7°, and 43.4° can be attributed to (012), (104), (110), and (202) crystal planes, confirming the successful preparation of Fe_2O_3 NPs. [22] The PXRD spectra of the synthesized PCN-224 represent peaks at 4.59°, 5.62°, 6.49°, and 7.96°, representing crystal planes (002), (112), (022), and (222), respectively, which are consistent with the XRD patterns reported for PCN-224. [23] PCN-224@Fe_2O_3 still retains the characteristic peaks of PCN-224 and Fe_2O_3 NPs (Figure S1A-B), suggesting the successful synthesis of PCN-224@Fe_2O_3. X-ray photoelectron spectroscopy (XPS) was utilized to investigate the chemical composition and bonding states of PCN-224@Fe_2O_3 composite. The XPS survey spectra in Fig. 1D confirm the presence of all characteristic elements of PCN-224 and Fe_2O_3 NPs in the composite. The high-resolution XPS spectrum of

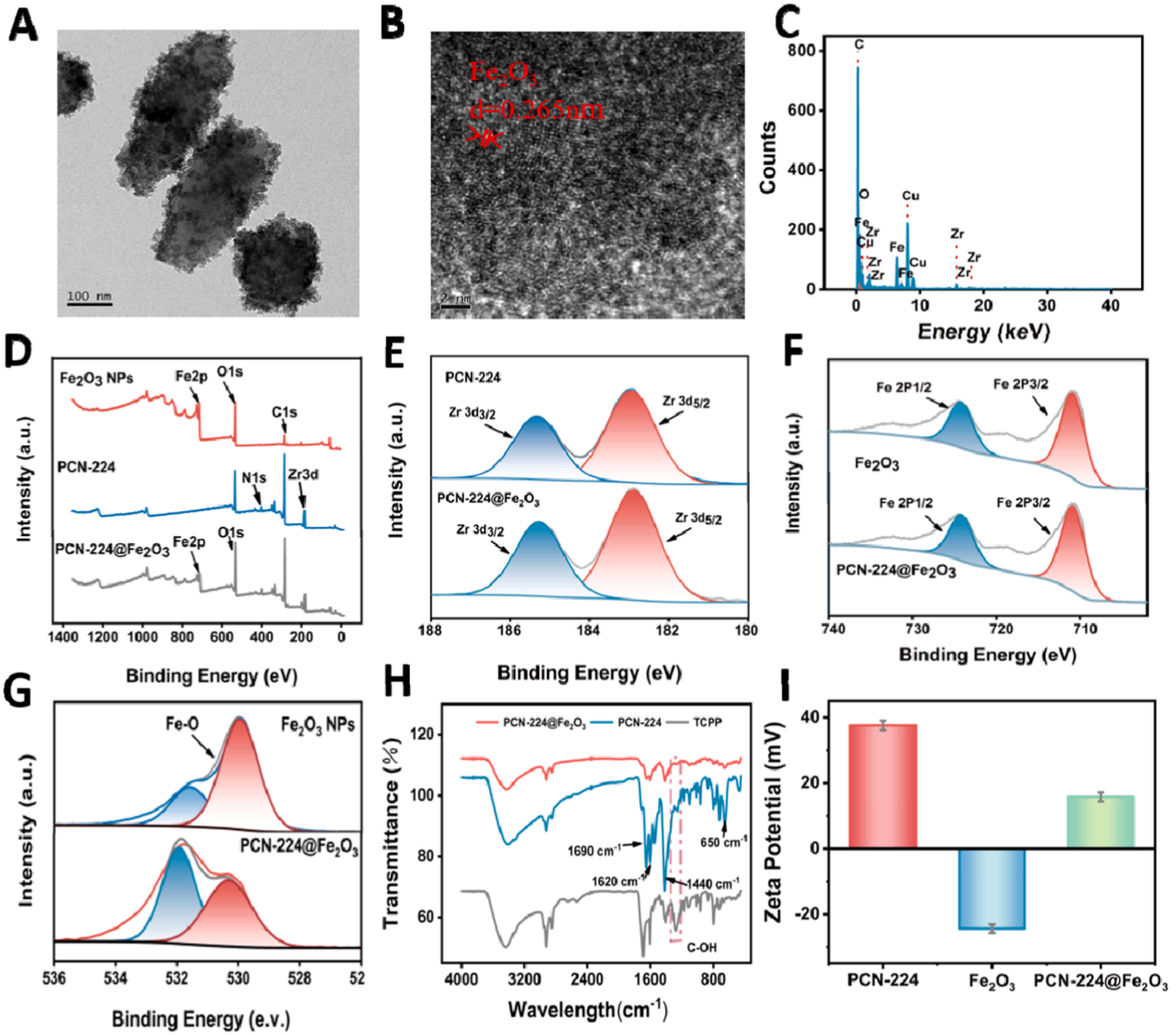

Fig. 1. (A) TEM, (B) high-resolution TEM images and (C) EDS spectrum of PCN-224@Fe_2O_3; (D) XPS spectra of Fe_2O_3, PCN-224, PCN-224@Fe_2O_3; XPS spectra of (E) Zr 3d in PCN-224 and PCN-224@Fe_2O_3, (F) Fe 2p in Fe_2O_3 and PCN-224@Fe_2O_3 and (G) O1s in Fe_2O_3 and PCN-224@Fe_2O_3; (H) FTIR spectra of TCPP, PCN-224 and PCN-224@Fe_2O_3; (I) Zeta potentials of PCN-224, Fe_2O_3 and PCN-224@Fe_2O_3.

Zr 3d in Fig. 1E shows specific peaks at 185.3 and 182.9 eV in PCN-224 and PCN-224@Fe_2O_3, respectively, indicating no structural or valence changes of PCN-224 after the in-situ growth of Fe_2O_3 [24]. Similarly, the binding energies of Fe 2P1/2 and Fe 2P3/2 in the PCN-224@Fe_2O_3 and Fe_2O_3 NPs were found to be analogous, as demonstrated in Fig. 1 F [25]. The XPS spectrum of O1s in Figure IG displays the characteristic peak of the Fe-O bond at 529.9 eV in Fe_2O_3 NPs, with a decrease in the proportion of Fe-O bonds in PCN-224@Fe_2O_3, indicating composite formation between PCN-224 and Fe_2O_3 NPs. In addition, considering that Fe element may enter the porphyrin ring structure to coordinate with N in the synthesis process to generate Fe-porphyrin, we analyzed the XPS spectra of N element in PCN-224 and PCN-224@Fe_2O_3 in detail (Figure S1C). PCN-224@Fe_2O_3 did not have a peak at 399.3 eV, which proved that Fe-porphyrin did not generate in the synthesis process. [26] FT-IR spectra of TCPP(Fe) and PCN-224@Fe_2O_3 were further compared to further validate this (Figure S1D). A distinct characteristic peak of Fe-N at 1004 cm^{-1} is observed in TCPP(Fe), indicating the incorporation of Fe^{3+} through metal ligand bond into the porphyrin ring. In contrast, the FT-IR spectrum of PCN-224@Fe_2O_3 does not exhibit the corresponding Fe-N bond peak at 1004 cm^{-1}, further confirming no Fe-porphyrin formation during the synthesis of PCN-224@Fe_2O_3. The FTIR spectrum in Fig. 1H shows prominent peaks at 1440 cm^{-1} for O-H bonds in PCN-224, peaks between 1620 and 1690 cm^{-1} attributed to C═O stretching coordinated with metal ions, peaks at 650 cm^{-1} for Zr-OH bonds and 1246 cm^{-1} for the asymmetric vibration absorption peak of C-OH, confirming the successful synthesis of PCN-224 and the unchanged structure after loading Fe_2O_3 NPs [27]. Zeta potential analysis (Fig. 1I) revealed positive charges on PCN-224 and negative charges of Fe_2O_3 NPs, suggesting composite formation possibly through electrostatic interaction. Taken together, these comprehensive analyses validate the successful synthesis of PCN-224@Fe_2O_3 [28].

As shown in the UV–vis spectra depicted in Figure S1E, the PCN-224@Fe_2O_3 composite also exhibits all the characteristic absorption peaks of PCN-224, with the peak positions remaining unchanged.

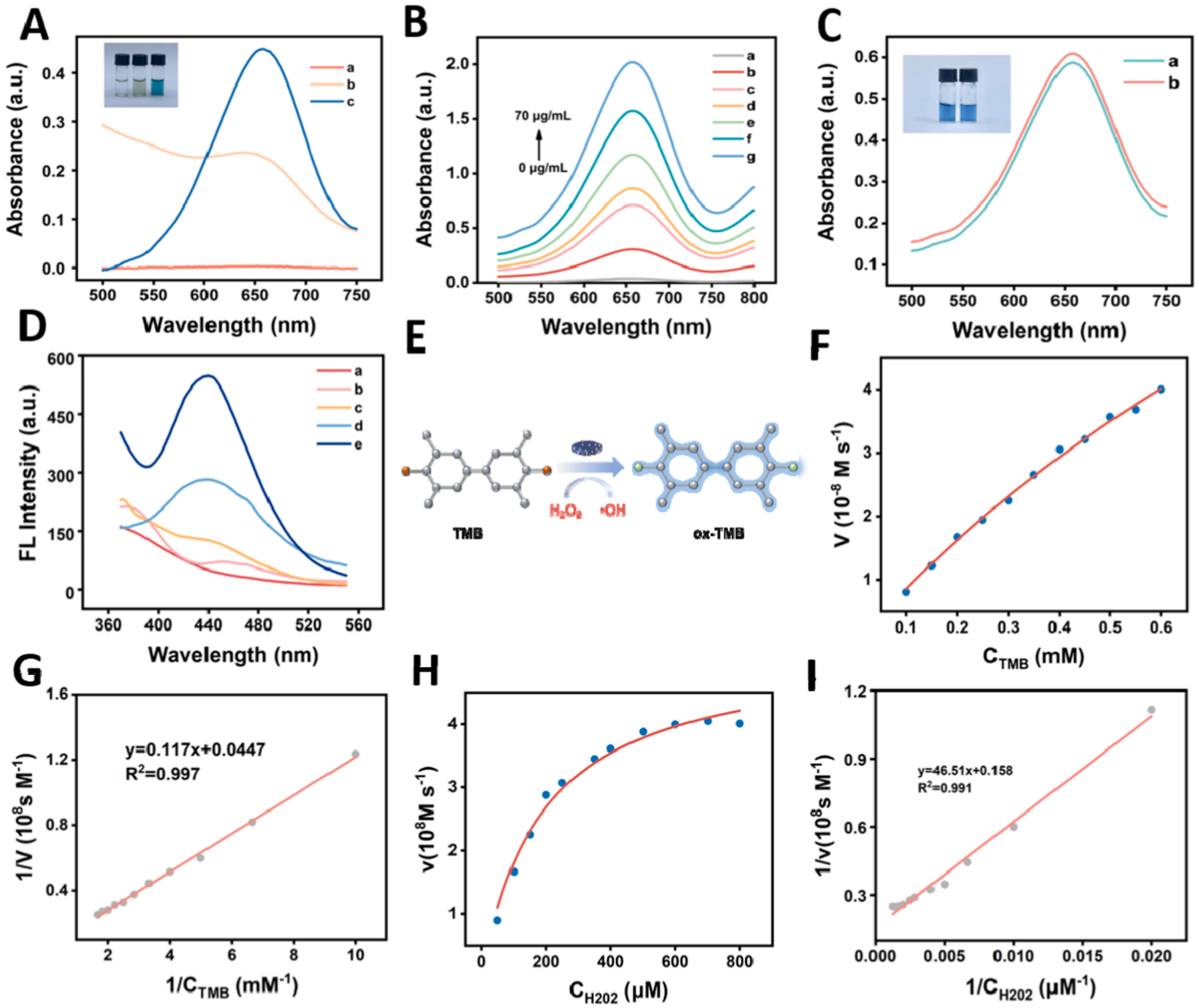

Fig. 2. (A) The verification of the POD-like activity of PCN-224@Fe_2O_3: (a) H_2O_2+TMB; (b) H_2O_2+TMB+Fe_2O_3; (c) H_2O_2+TMB+PCN-224@Fe_2O_3. (B) Effect of catalyst concentration (0, 10, 20, 30, 40, 50, 60, 70 μg/mL). (C) The UV absorbance of TMB in N_2 and air conditions; (D) Testify of the exist of ·OH generated by PCN-224@Fe_2O_3 react with H_2O_2. (a) TA; (b) TA+PCN-224@Fe_2O_3; (c) TA+H_2O_2; (d) TA+H_2O_2+Fe_2O_3 (e) TA+H_2O_2+PCN-224@Fe_2O_3. (E) Schematic illustration colorimetric reaction principle of TMB using PCN-224@Fe_2O_3 as the catalyst. The relationship between velocity (v) and the concentration of the substrate of TMB (F) and H_2O_2 (H). The double-reciprocal plots for TMB (G) and H_2O_2 (I). Experimental conditions: pH 4.5; 50 μg/mL PCN-224@Fe_2O_3; 10 mM H_2O_2 and 0.40 mM TMB; incubated at 35 ℃ for 30 min.

Fluorescence spectroscopy, shown in Figure S1F, reveals that PCN-224 exhibits pronounced fluorescence properties, which is significantly quenched after loading Fe_2O_3, indicating effective incorporation of Fe_2O_3 onto the PCN-224 framework.

3.2. Kinetic studies of the peroxidase activity of the PCN-224@Fe_2O_3

The POD-like activity of PCN-224@Fe_2O_3 has been investigated using TMB and H_2O_2 as substrates. The catalyst facilitates the oxidation of TMB, resulting in the formation of a blue oxidized form known as ox-TMB. A comparative analysis in Fig. 2 A and S2A shows the improved catalytic performance of PCN-224@Fe_2O_3 compared to Fe_2O_3 under identical conditions and mass concentration. The POD-like activity of PCN-224@Fe_2O_3 with different PCN-224 and $FeCl_3$ ratios was tested, and the results showed that the best POD-like activity was obtained when the mass concentration ratio of PCN-224 to $FeCl_3$ was 3:4. The presence of Fe_2O_3 NPs is critical for inducing the color change in the TMB solution, as PCN-224 alone does not exhibit this effect (Figure S2A). The enhanced POD-like activity of PCN-224@Fe_2O_3 is attributed to the Fe_2O_3 NPs electrostatically interacting with the PCN-224 surface, thereby increasing the local concentration of active iron sites for the subtract interaction [29]. The highly porous structure of PCN-224 also facilitates efficient mass transfer of TMB, H_2O_2, and their reaction intermediates. The concentration of PCN-224@Fe_2O_3 affects the absorption peak at 652 nm, as shown in Fig. 2B. The role of oxygen in the catalytic process is minimal, as shown in Fig. 2 C. Furthermore, the optimal pH for better POD-like activity of PCN-224@Fe_2O_3 is determined at pH 4.5, with negligible OXD-like activity of PCN-224@Fe_2O_3 observed (Figure S2B). Examination of the catalytic mechanism in Fig. 2D reveals the generation of ·OH intermediates, which is confirmed by the formation of the fluorescent species of TAOH by the reaction of TA probe with ·OH. [30] The PCN-224@Fe_2O_3 demonstrates superior POD-like activity by producing more ·OH compared to Fe_2O_3 NPs under equivalent conditions and mass concentration. The main mechanism diagram is depicted in Fig. 2E. K_m is a key indicator of the affinity between enzymes and substrates, where a lower K_m value indicates a better affinity to the substrate. Under optimal conditions of pH 4.5 and temperature of 35 °C (Figure S5), steady-state kinetic experiments were performed to determine the kinetic constants of PCN-224@Fe_2O_3 in Fig. 2F-I, including the Michaelis constant K_m and the maximum reaction rate V_{max}. By varying the concentrations of TMB and H_2O_2 and fitting the initial reaction rate values and substrate concentrations, Michaelis-Menten curves and Lineweaver-Burk plots were obtained. The Lineweaver-Burk plot in Fig. 2 G shows a linear regression equation for TMB as $y = 0.117x + 0.0447$ ($R^2 = 0.997$), with K_m and V_{max} values of 2.617 mM and 2.237×10^{-7} M s^{-1}, respectively. The linear regression equation for H_2O_2 is $y = 46.51X + 0.158$ ($R^2 = 0.991$), with K_m and V_{max} values of 0.29 mM and 6.32×10^{-8} M s^{-1}, respectively (Fig. 2I). Additionally, for comparison, the catalytic kinetics of Fe_2O_3 NPs were investigated (Figure S3). Table S1 provides a clear comparison of V_{max} and K_m between Fe_2O_3 NPs and PCN-224@Fe_2O_3, showing that PCN-224@Fe_2O_3 has a higher V_{max} and a lower K_m. This improved performance is further validated by comparisons with natural peroxidase and other POD-like nanozymes, confirming the commendable affinity of PCN-224@Fe_2O_3 towards H_2O_2 and TMB. The exceptional POD-like activity of PCN-224@Fe_2O_3, which is attributed to the unique structure properties of PCN-224 that facilitate the loading of Fe_2O_3 NPs and enhanced mass transfer, paves the way for the development of a colorimetric sensing platform utilizing its POD-like activity. In addition, the distinctive red fluorescence property exhibited by the PCN-224 makes it suitable for fluorescence analysis, thus enabling a colorimetric/fluorescence dual-mode detection platform.

3.3. Dual-channel detection of ATP by colorimetric and fluorescence

The incorporation of Fe_2O_3 onto PCN-224 has been demonstrated with enhanced POD-like activity as a nanozymes, accompanying with significant decrease in fluorescence of PCN-224. Previous studies have shown that the phosphate has a strong affinity to Zr present in PCN-224, potentially affecting the optical properties of the material. [31] The molecular structure of adenosine triphosphate (ATP), consisting of an adenine ring, ribose, and a triphosphate group, is believed to play a role in regulating the mimic activity and fluorescence properties of PCN-224@Fe_2O_3. Experimental results, shown in Figure S4A, demonstrate a decrease in the UV–vis absorbance peak at 652 nm with increasing ATP concentration. This can be attributed to the interaction of ATP with PCN-224@Fe_2O_3 through Zr-O-P bonds, causing structural changes in PCN-224@Fe_2O_3 and a subsequent decrease in POD-like activity. Interestingly, ATP itself does not exhibit POD-like behavior under the similar experimental conditions (Figure S2B). Furthermore, Figure S4B shows that the fluorescence PCN-224@Fe_2O_3 is enhanced with the introduction of ATP. These results support the notion of a dual-channel detection approach for ATP using UV spectroscopy and fluorescence, underscoring the validity of our proposed hypothesis.

Under these optimized conditions, ATP was detected via the POD-like activity of PCN-224@Fe_2O_3 using the colorimetric method. Fig. 3 A clearly shows that with the introduction of ATP, the UV absorption peak at 652 nm consistently decreased in the concentration range of 10^{-4}-100 μM. Notably, there is a robust linear correlation between the logarithmic concentration of ATP and the absorbance peak at 652 nm, described by the equation of $A = -0.048 \log[ATP] + 0.197$ ($R^2 = 0.997$), with a remarkable detection limit of 29 pM (S/N = 3) for ATP (Fig. 3A-B).

The conditions for fluorescence detection of ATP were optimized, including parameters of pH, temperature, time, and the concentration of PCN-224@Fe_2O_3 (Figure S6). The results indicated that the most favorable conditions for the reaction included pH 7.5, temperature of 50 °C, reaction time of 50 min, and material concentration of 50 μg/mL. Under these optimized experimental settings, the detection of ATP by fluorescence analysis was successfully achieved, as shown in Fig. 3D-E. The established linear relationship, represented by $Y = 422.95 \log [ATP] + 287.59$ ($R^2 = 0.997$) in the range of 0.8–100 μM, showed a detection limit of 0.78 μM. We also conducted the detection of ATP at 25 °C using fluorescence method, as shown in Figure S7A-B, a linear relationship was also obtained in 0.8–60 μM with the equation of $Y = 43.33 \log [ATP] + 259.63$ ($R^2 = 0.989$). These results indicated that the detection of ATP at 50 °C achieved higher detection sensitivity, which may result from the accelerated molecular motion at higher temperature and the less detachment after the attachment of ATP on the surface of PCN-224@Fe_2O_3. [32]

The design discussed in this context demonstrates notable sensitivity, achieved through the utilization of dual-channel detection employing fluorescence and colorimetric methods. This approach not only offers mutual validation but also exhibits superior performance compared to other techniques, as shown in Table S2. The selectivity of this detection platform towards ATP was rigorously confirmed by evaluating potential interfering substances, including Na^+, NH_4^+, Zn^{2+}, Ca^{2+}, Fe^{2+}, Cys, GSH, DA, and AA (Fig. 3 C, F), revealing minimal response in both fluorescence and UV–vis analysis. This underscores the excellent specificity in ATP detection. The distinctive mechanisms underlying UV–vis and fluorescence detection, modulated by the interaction of ATP and PCN-224@Fe_2O_3, enable independent and varying sensitivities in the two modes. Consequently, researchers are afforded the flexibility to choose either or both modes of output to ensure precise and dependable quantification of ATP in accordance with specific experimental requirements.

3.4. Study on the mechanism of ATP detection

The TEM image of PCN-224@Fe_2O_3 after ATP addition is shown in Fig. 4 A, which shows a degree of aggregation after ATP addition. EDX (Figure S8A) and elemental mapping (Fig. 4B) of the ATP-treated PCN-

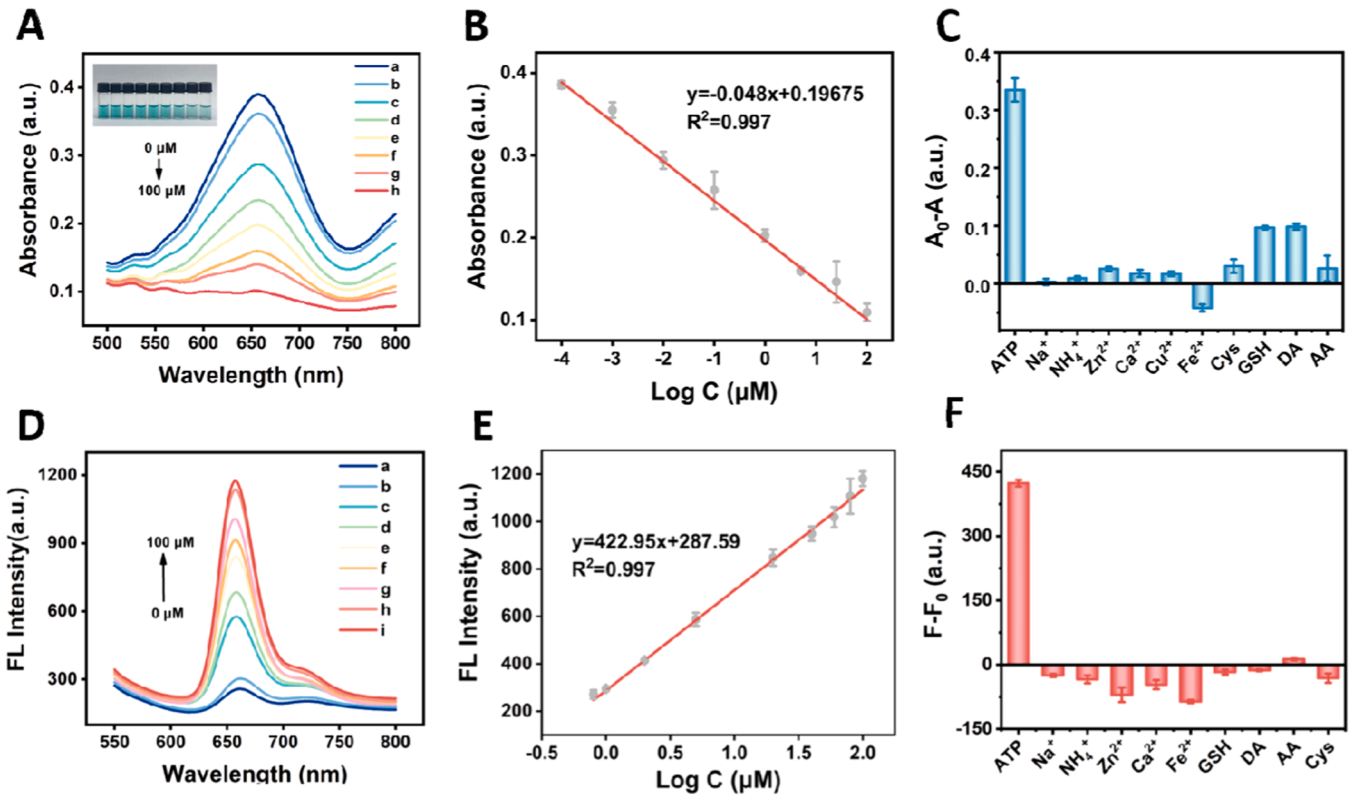

Fig. 3. (A) Colorimetric determination of ATP (0.1 nM-100 μM) and (B) the corresponding calibration curve; (C) Selectivity of the colorimetric sensing of ATP (ATP: 10 μM, other interferences: 50 μM). Experimental conditions: pH 4.5; 50 μg/mL PCN-224@Fe_2O_3; 10 mM H_2O_2 and 0.40 mM TMB; incubated at 35 ℃ for 30 min. (D) Fluorescence method determination of ATP in the mixture of PCN-224@Fe_2O_3 with various ATP concentrations (0.8–100 μM) and (E) the corresponding calibration curve for ATP (0.8–100 μM); (F) Selectivity of the fluorescence sensing method for ATP (ATP: 10 μM, other interferences: 50 μM). Experimental conditions: pH 7.5; 50 μg/mL PCN-224@Fe_2O_3; incubated at 50 ℃ for 50 min.

224@Fe_2O_3 showed characteristic peaks of Zr, Fe, O, N, C and P elements. The presence of phosphorus, a characteristic element of ATP, suggests the specific interaction between ATP and PCN-224@Fe_2O_3. In addition, the elemental mapping images illustrated a closely overlapping dispersion area of Zr and P elements on the composite, indicating potential reaction sites of P and Zr elements within PCN-224@Fe_2O_3. Zeta potential analysis in Fig. 4 C indicate that PCN-224@Fe_2O_3 carries positive charges, while ATP is negatively charged, facilitating their interaction through electrostatic forces. Subsequently, the POD-like activity of ATP-treated Fe_2O_3 NPs in Fig. 4D was significantly reduced compared to untreated Fe_2O_3 NPs [33], suggesting an interaction between ATP and Fe_2O_3 NPs. [34] The FT-IR spectra analysis of PCN-224@Fe_2O_3 before and after ATP addition (Figure S8B) reveals the formation of Zr-O-P bonds between ATP and Zr elements, indicated by a distinct bond appearing of at 1055 cm^{-1}. [35] Moreover, the XPS analysis of PCN-224@Fe_2O_3 after ATP addition (Fig. 4E-J) further elucidated the interaction mechanism. This is evidenced by the disappearance of Zr^{4+} peaks and the emergence of Zr-O-P bonding peaks at 190.0 eV. Particularly, the XPS spectrum of the PCN-224@Fe_2O_3-ATP (Fig. 4E) displays a novel peak with the binding energy of 133.9 eV, attributable to P2p from the ATP. [36] These findings are prominently highlighted in the high-resolution XPS spectra of P 2p in Fig. 4I. The relative content of Zr and Fe elements decreased compared to the C elements after ATP addition, indicating the coordination between ATP, Zr, and Fe_2O_3 NPs. This interaction altered the structure of PCN-224@Fe_2O_3, resulting in a decrease in the number of activity sites and the transport of substances within the pores of PCN-224, thus reducing the POD-like activity of PCN-224@Fe_2O_3. Additionally, as shown in Figure S8C, the fluorescence of the supernatant experienced an increase subsequent to the introduction of ATP and centrifugation of the system. This phenomenon could potentially imply the liberation of certain TCPP ligands, suggesting a weakening in the Zr-TCPP interaction due to the binding of ATP-PCN-224@Fe_2O_3. To substantiate the release of TCPP, high resolution mass spectrometry (HR-MS) was employed to characterize the supernatant of PCN-224@Fe_2O_3 after the addition of ATP. Given the presence of four carboxyl groups within the porphyrin structure, it is plausible that the hydrogen in these groups could ionize in negative ion mode. Notably, as illustrated in Figure S8D, the presence of a peak at 786.7736 signifies the existence of TCPP in the supernatant, consequently providing further validation regarding the release of TCPP and the structural modification of PCN-224@Fe_2O_3. Therefore, the structure of PCN-224@Fe_2O_3 is partially changed by ATP, forming the Zr-O-P bonds on the surface, and releasing TCPP with enhanced fluorescence. The decrease of the exposed active Fe_2O_3 NPs further contributed to the reduction of POD-like activity of PCN-224@Fe_2O_3.

3.5. Dual-channel detection of Cu^{2+} by colorimetry and fluorescence

The detection of Cu^{2+} was based on the PCN-224@Fe_2O_3 system after the introduction of ATP, which was driven by the remarkable coordination interaction observed between Cu^{2+} and ATP. [37] Upon the introduction of Cu^{2+}, the POD-like activity was restored, possibly due to the interaction between ATP and Cu^{2+}, which could weaken the interaction of PCN-224@Fe_2O_3 and ATP, as shown in Figure S9A, thus restoring the POD-like activity of PCN-224@Fe_2O_3. By optimizing the detection conditions for Cu^{2+}, particularly the concentration of ATP, an optimal ATP concentration of 50 μM was determined (Figure S9C). Under the optimized conditions, as shown in Fig. 5 A, a gradual increase in the UV peak at 652 nm was observed with increasing concentration of Cu^{2+}. A good linear equation $A = 0.007\ [Cu^{2+}] + 0.166$ ($R^2 = 0.991$) was obtained within 0.1–25 μM, with a detection limit of 91 nM (S/N = 3) (Fig. 5B), surpassing other existing methods in terms of sensitivity

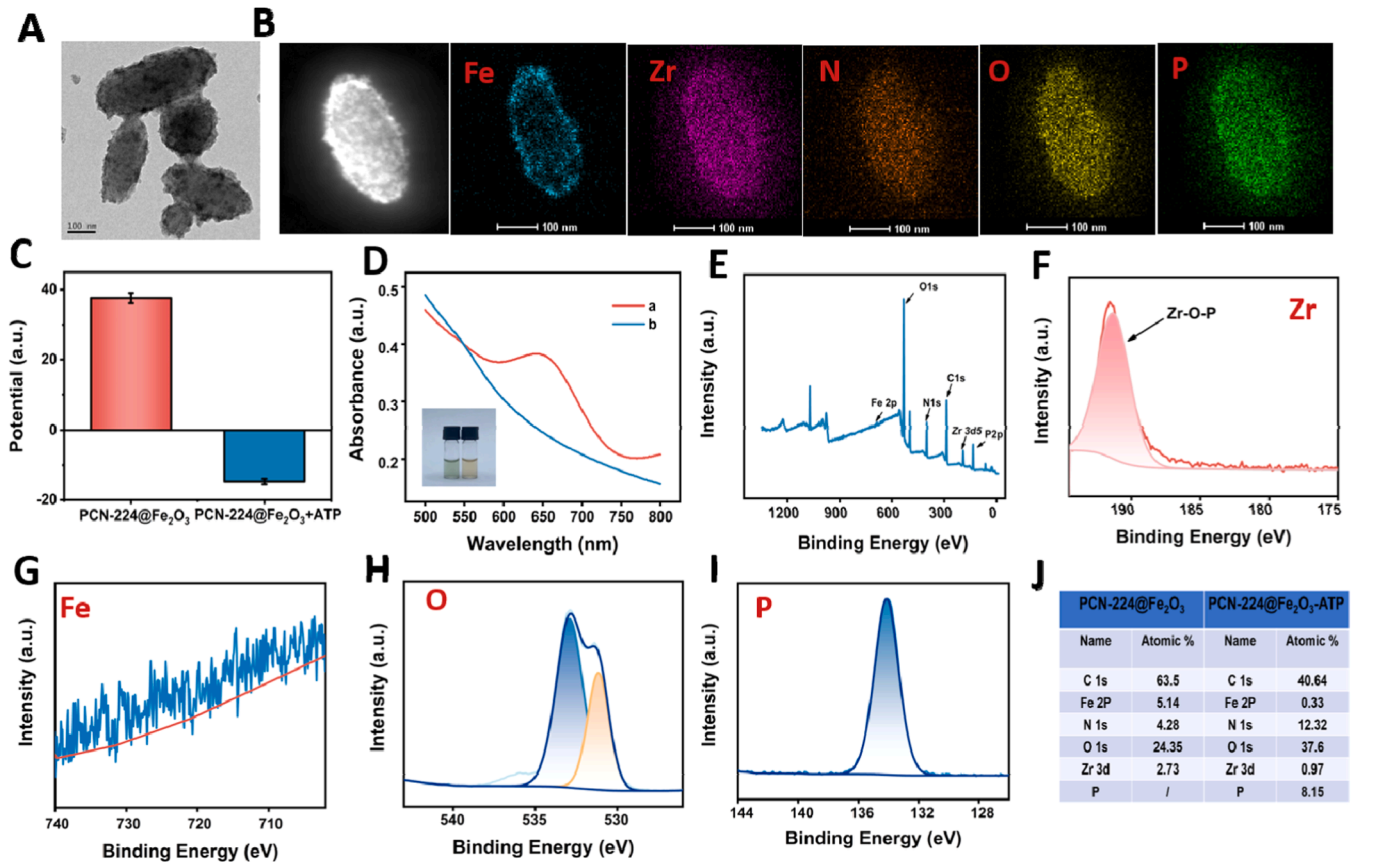

PCN-224@Fe_2O_3		PCN-224@Fe_2O_3-ATP	
Name	Atomic %	Name	Atomic %
C 1s	63.5	C 1s	40.64
Fe 2P	5.14	Fe 2P	0.33
N 1s	4.28	N 1s	12.32
O 1s	24.35	O 1s	37.6
Zr 3d	2.73	Zr 3d	0.97
P	/	P	8.15

Fig. 4. (A) TEM and (B) element mapping images of PCN-224@Fe_2O_3 after adding ATP; (C) Zeta potentials of Fe_2O_3@PCN-224, Fe_2O_3@PCN-224+ATP. (D) The UV absorbance of TMB in the absence and presence of ATP in Fe_2O_3 solution (a: without ATP; b: with ATP); (E) XPS spectrum of PCN-224@Fe_2O_3-ATP and their corresponding high-resolution spectra of (F) Zr; (G) Fe; (H) O; (I) N in PCN-224@Fe_2O_3+ATP. (J) The element contents of PCN-224@Fe_2O_3 and PCN-224@Fe_2O_3-ATP.

(Table S3).

Furthermore, the introduction of Cu^{2+} results in the quenching of the fluorescence at 650 nm, providing a second channel for Cu^{2+} detection. By fine-tuning the ATP amount and the reaction time, optimal conditions for Cu^{2+} detection by fluorescence were achieved (Figure S9B). Notably, the best quenching effect of Cu^{2+} was achieved with 50 μM ATP, which can be reached stable within 10 minutes after Cu^{2+} addition (Figure S9D-E). Under the optimal conditions, in the range of 0.1–25 μM, a good linear relationship of $F = -22.942 \log[Cu^{2+}] + 839.290$ ($R^2 = 0.992$) was obtained with a detection limit of 92 nM (S/N = 3) (Fig. 5D-E), outperforming most existing methods (Table S3). To demonstrate the selectivity of this platform in the detection of Cu^{2+}, the colorimetric and fluorescence dual-mode sensing approach using PCN-224@Fe_2O_3 was employed to investigate potential interferences. The response of Na^+, NH_4^+, Ca^{2+}, Ba^{2+}, Mg^{2+}, Pb^{2+}, Ag^+, Mn^{2+}, Mg^{2+} at a concentration of 50 μM was carefully investigated. Compared with the response to Cu^{2+} at 10 μM, the effect of other substances was found to be minimal, suggesting that this method has excellent selectivity for the detection of Cu^{2+} (Fig. 5 C, F).

3.6. Study on the mechanism of Cu^{2+} detection

To illustrate the detection mechanism of Cu^{2+}, FTIR and Zeta potential analysis were performed after the addition of Cu^{2+} ions. The FTIR spectrum shown in Figure S10A displayed a decrease in the intensity of the stretching vibration of Zr-O-P bonds in the range of 900 and 1200 cm^{-1} in PCN-224@Fe_2O_3-ATP after the addition of Cu^{2+}. [38] This attenuation can be attributed to the complexation affinity between ATP and Cu^{2+}, which causes repulsion of ATP from the PCN-224@Fe_2O_3. Zeta potential measurements (Figure S10B) confirmed that the positively charged Cu^{2+} did affected the potential of the PCN-224@Fe_2O_3-ATP system. Furthermore, the impact of Cu^{2+} introduction on the POD-like activity of the Fe_2O_3 NPs-ATP system was investigated. The UV-Vis spectrum in Figure S10C clearly showed that the incorporation Cu^{2+} resulted in a partial restoration of the POD-like activity of Fe_2O_3 NPs, indicating a weakening of the interaction between ATP and the active sites of Fe_2O_3 NPs and PCN-224@Fe_2O_3, thereby restoring the POD-like activity of PCN-224@Fe_2O_3. Due to Cu^{2+} itself has Fenton effect, the effect of Cu^{2+} on the UV absorption peak at 652 nm was investigated. It can be seen from Figure S11D that the Fenton effect of Cu^{2+} itself does not does not have a significant influence on the detection of Cu^{2+} in this system through its Fenton effect alone. Additionally, the fluorescence spectra in Figure S10D-F confirmed the suppression of fluorescence by Cu^{2+} potentially due to the quenching ability of Cu^{2+} toward PCN-224 or the released TCPP. To confirm this, the effect of Cu^{2+} on the fluorescence of PCN-224 itself was also examined, which showed a decrease in fluorescence intensity with increasing of Cu^{2+}, as shown in Figure S11F. As shown in Fig. S10C, regardless of whether copper ions were introduced into PCN-224-ATP or PCN-224@Fe_2O_3-ATP, the fluorescence in the supernatant was partially quenched, indicating the ability of copper ions to quench the fluorescence of TCPP. Taken together, these results suggest that the suppression of fluorescence by Cu^{2+} may involve interactions of Cu^{2+} with the released TCPP and the PCN-224 [39]. Thus, the proposed detection platform shows a signal amplification effect compared to using PCN-224 detection.

The experiments have successfully validated the mechanism by which positively charged Cu^{2+} ions interact with PCN-224@Fe_2O_3-ATP,

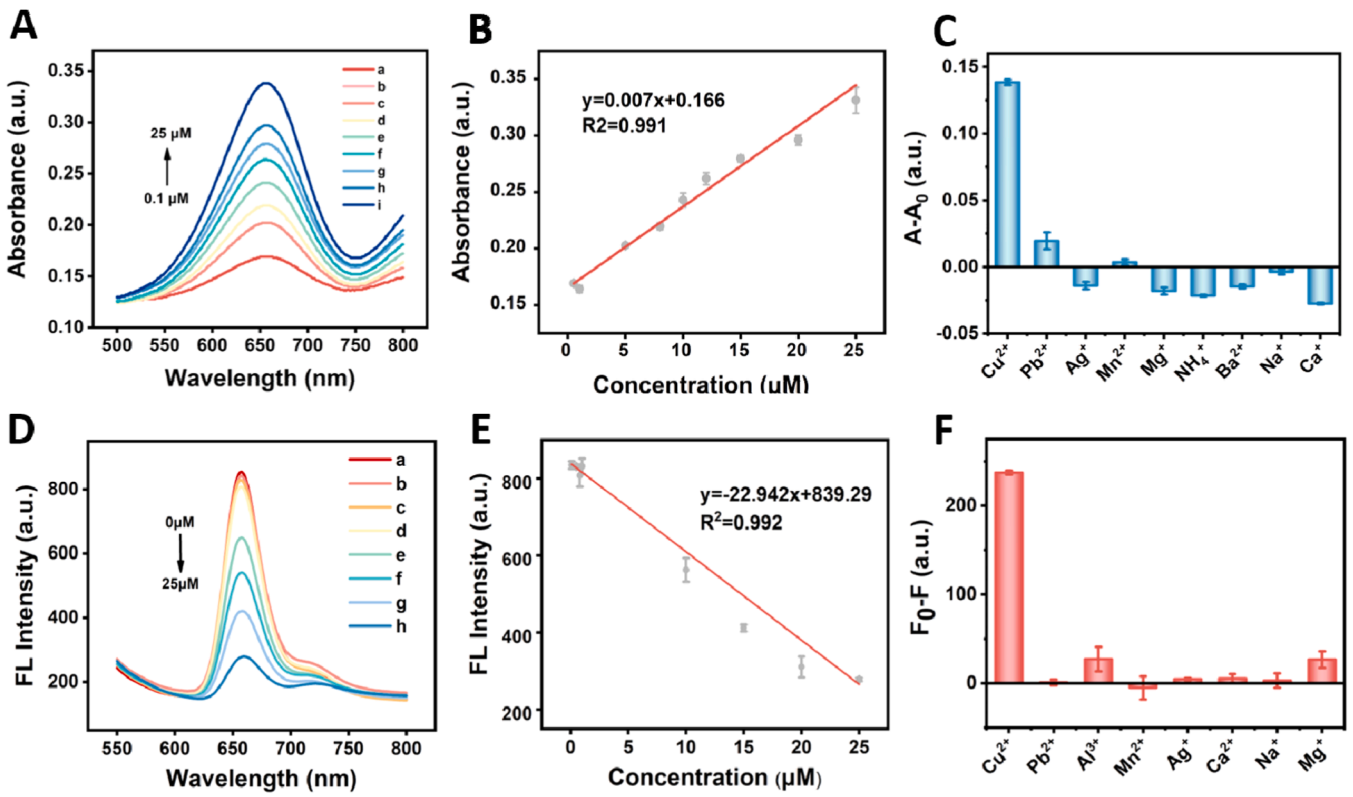

Fig. 5. (A) Colorimetric determination of Cu^{2+} (0.1–25 μM) and the (B) corresponding calibration curve for Cu^{2+} detection; (C) Selectivity for Cu^{2+} sensing (Cu^{2+}: 10 μM, other interferences: 50 μM) via colorimetric method based on the POD-like activity of PCN-224@Fe_2O_3. Experimental conditions: pH 4.5; 50 μg/mL PCN-224@ Fe_2O_3; 10 mM H_2O_2 and 0.40 mM TMB; incubated at 35 ℃ for 30 min. (D) Fluorescence spectra of PCN-224@Fe_2O_3 +ATP with various Cu^{2+} concentrations (0–25 μM), and (E) the calibration curve for Cu^{2+} (0.1–25 μM); (F) Selectivity testing via the fluorometric method (Cu^{2+}: 10 μM, other interferences: 50 μM). Experimental conditions: pH 7.5; 50 μg/mL PCN-224@ Fe_2O_3; incubated at 50 ℃ for 60 min.

leading to the weakening of Zr-O-P bonds and consequently enhancing the mimic activity of PCN-224@Fe_2O_3 by increasing the active sites of Fe_2O_3. Additionally, Cu^{2+} was observed to interact with TCPP and the PCN-224, resulting in the quenching of fluorescence in the system. The dual-channel detection of ATP and Cu^{2+} based on the strategy of regulating the activity of oxide nanozymes using the multifunctional PCN-224 as a carrier and the specific interaction to increase the selectivity. This approach can create an optimized microenvironment for tuning the mimic activity of nanozymes and facilitate the construction of a dual-mode sensing platform.

3.7. Actual sample analysis

In the assessment of the feasibility of PCN-224@Fe_2O_3, we utilized colorimetric and fluorescence dual-mode sensing techniques to quantify the levels of ATP and Cu^{2+} in human serum samples and Cu^{2+} in tap water. To enhance the reliability of the sensing platform for continuous detection, we investigated ATP detection subsequent to Cu^{2+} masking using EDTA as the masking agent. Figure S12 illustrates that the impact of EDTA on the fluorescence of PCN-224@Fe_2O_3 and PCN-224@Fe_2O_3-ATP can be disregarded upon the introduction of 40 μM EDTA. Our comparison of fluorescence readings with and without the presence of

Table 1
Detecting ATP and copper ions in actual samples.

Detection object	Detection method	Sample Found		Added (μM)	Detected (μM)	recovery (%, n=3)	RSD (%, n=3)
ATP	Fluorescence	Serum	Not Found	0.80	0.72	90.00	3.69
				5.00	4.97	99.40	4.88
				20.00	21.80	109.00	8.99
	UV–vis	Serum	Not Found	0.50	0.51	102.00	0.67
				5.00	5.34	106.80	0.57
				50.00	45.84	91.70	1.41
Cu^{2+}	Fluorescence	Serum	Not Found	0.50	0.54	108.00	5.37
				5.00	4.53	90.60	1.56
				15.00	15.47	103.10	2.70
	UV–vis	Serum	Not Found	0.50	0.46	92.00	2.46
				5.00	5.12	102.40	2.99
				15.00	15.74	104.90	3.16
Cu^{2+}	Fluorescence	Tap Water	Not Found	0.50	0.48	96.00	2.53
				5.00	5.46	109.20	1.67
				20.00	19.70	98.50	4.54
	UV–vis	Tap Water	Not Found	0.50	0.53	106.00	1.41
				5.00	5.05	101.00	2.52
				20.00	19.70	98.50	1.53

copper ions (depicted in red and light blue) demonstrated significant interference from copper ions on ATP detection. We proceeded to evaluate the fluorescence responses of ATP subsequent to Cu^{2+} masking with EDTA, revealing no discernible differences in ATP detection under the same conditions, regardless of the presence of copper ion interference. Notably, the order of EDTA addition did not alter the outcomes, affirming the efficacy of EDTA in mitigating copper ion interference in ATP detection (Figure S12).

The results presented in Table 1 show that the recovery rates of spiked ATP in serum were 91.7–106 % and 90.6–109.2 % when assessed by UV and fluorescence methods, respectively. Similarly, the recovery rates of the spiked Cu^{2+} in tap water and serum were 96.0–109.2 % and 90.6–108 % via UV and fluorescence detection methods, respectively. These results underscore the reliability of the sensing platform in detecting ATP and Cu^{2+} in real samples. Both techniques showed high sensitivity in analyzing the targets due to the exceptional POD-like properties of PCN-224@Fe_2O_3, the runnable fluorescence properties of PCN-224, and the structural change induced by the targets. In addition, the results obtained from both methods were in concordance, highlighting the importance of selecting appropriate analytical approaches for sample analysis and validation by dual methods to avoid erroneous results.

4. Conclusions

PCN-224@Fe_2O_3 was synthesized through a facile two-step hydrothermal method, which exhibited enhanced POD-like activity and weak fluorescence. The multifunctional PCN-224 not only acts as the supporter but creates a microenvironment for tuning the mimic activity of nanozymes and facilitates the construction of a dual-mode sensing platform. The in-situ growth of Fe_2O_3 NPs onto PCN-224 significantly increases the number of active sites and local catalyst concentration. The exceptional surface area and porous structure of PCN-224 facilitate efficient mass transfer of reactants and intermediates, thereby boosting the POD-like activity. The composite demonstrates the ability to continuously detect ATP and copper ions via the fluorescence/UV–vis dual-channel approach due to the sensitive structural changes in PCN-224@Fe_2O_3. The fluorescence properties of PCN-224 was quenched after loading of Fe_2O_3 NPs, enabling sequential detection of ATP and Cu^{2+} by inducing microenvironment changes through specific interactions with the PCN-224@Fe_2O_3. This dual-channel platform is sensitive, fast, selective, and successfully applied in real sample analysis. This strategy of tuning nanozyme-like properties of metal oxide nanomaterials with fluorescence MOFs holds great promise for the development of versatile dual-channel and multifunctional nanoplatforms with applications in disease diagnosis, environmental monitoring, and food analysis.

CRediT authorship contribution statement

Feng Liu: Visualization, Methodology. **Mingjie Wei:** Supervision, Resources, Methodology. **Meiling Liu:** Writing – review & editing, Supervision, Project administration, Funding acquisition, Conceptualization. **Shouzhuo Yao:** Supervision. **Xiaohua Zhu:** Validation, Software, Project administration. **Youyu Zhang:** Supervision, Conceptualization. **Lin Chai:** Validation, Software, Investigation. **Jing Liu:** Software, Formal analysis. **Yani Liu:** Writing – original draft, Validation, Software, Investigation, Formal analysis, Data curation. **Haoyu Chen:** Validation, Software, Methodology, Investigation, Formal analysis. **Shu Huang:** Resources, Project administration, Methodology.

Declaration of Competing Interest

The authors declare that they have no known competing financial interests or personal relationships that could have appeared to influence the work reported in this paper.

Data availability

Data will be made available on request.

Acknowledgements

This work was financially supported by the National Natural Science Foundation of China (22274047, 21974042, 22274048), the Science and Technology Department of Hunan Province (2021JJ30012), the Hubei Science and Technology Program (2022CFB781).

Supplementary information

XRD, XPS, FT-IR, UV–vis absorbance and fluorescence characterization of the materials; Effect of the proportions of PCN-224 and Fe_2O_3, OXD-like activity of PCN-224@Fe_2O_3 and POD-like activity of ATP; Kinetic studies of the peroxidase-like activity of the PCN-224@Fe_2O_3; Feasibility for dual-channel detection of ATP by colorimetric and fluorescence methods; Effects on the POD-like activity of PCN-224@Fe_2O_3; Optimization of the detection in fluorescence method; Fluorescence detection of ATP at 25 ℃ based on PCN-224@Fe_2O_3; Detection (ATP) mechanism confirmation; Feasibility for dual-channel detection of Cu^{2+} by colorimetric and fluorescence, and the optimization of the detection conditions; Detection (Cu^{2+}) mechanism confirmation; Confirmation the effect of Fenton reaction of copper ions; The detection of ATP after masking Cu^{2+} ions; Comparison of the K_m and V_{max} of PCN-224@Fe_2O_3 with HRP and other nanozymes; Comparison of ATP detection with different optical methods; Comparison of Cu^{2+} detection with different methods.

This supplementary information is available free of charge on the website.

Appendix A. Supporting information

Supplementary data associated with this article can be found in the online version at doi:10.1016/j.snb.2024.136226.

References

[1] J.S. Swensen, Y. Xiao, B.S. Ferguson, A.A. Lubin, R.Y. Lai, A.J. Heeger, K.W. Plaxco, H.T. Soh, Continuous, real-time monitoring of cocaine in undiluted blood serum via a microfluidic, electrochemical aptamer-based sensor, J. Am. Chem. Soc. 131 (12) (2009) 4262–4266, https://doi.org/10.1021/ja806531z.

[2] J. Oh, C. Min, D. Park, M.S. Han, Oligonucleotide-chemosensor conjugate as a dual responsive detection platform and its application for simultaneous detection of ATP and Zn^{2+}, ACS Sens 7 (12) (2022) 3933–3939, https://doi.org/10.1021/acssensors.2c02006.

[3] J. You, S. Lee, H.J. Tark, M.J. Nang, J.H. Oh, I. Choi, Optical detection of copper ions structural dissociation of plasmonic sugar nanoprobes, Anal. Chem. 94 (14) (2022) 5521–5529, https://doi.org/10.1021/acs.analchem.1c04340.

[4] F. Shi, Y. Li, Z. Lin, D. Ma, X. Su, A novel fluorescent probe for adenosine 5′-triphosphate detection based on Zn^{2+}-modulated l-cysteine capped cdte quantum dots, Sens. Actuators, B 220 (2015) 433–440, https://doi.org/10.1016/j.snb.2015.05.087.

[5] X. Jin, J. Gao, P. Xie, M. Yu, T. Wang, H. Zhou, A. Ma, Q. Wang, X. Leng, X. Zhang, Dual-functional probe based on rhodamine for sequential Cu^{2+} and ATP detection in vivo, Spectrochim. Acta A 204 (2018) 657–664, https://doi.org/10.1016/j.saa.2018.06.094.

[6] S. Hu, X. Li, K. Wang, Q. Wu, G. Zhang, X. Liu, Sensor array based on carbon dots for ATP-related physiological phosphates detecting and ATP hydrolysis monitoring, Sens. Actuators, B 310 (2020), https://doi.org/10.1016/j.snb.2020.127851.

[7] L.L. Lu, R.J. Zeng, Q.Y. Lin, X. Huang, D.P. Tang, Cation exchange reaction-mediated photothermal and polarity-switchable photoelectrochemical dual-readout biosensor, Anal. Chem. 95 (44) (2023) 16335–16342, https://doi.org/10.1021/acs.analchem.3c03573.

[8] X. Liao, B. Wu, H. Li, M. Zhang, M. Cai, B. Lang, Z. Wu, F. Wang, J. Sun, P. Zhou, H. Chen, D. Di, C. Ren, H. Zhang, Fluorescent/Colorimetric dual-mode discriminating gln and val enantiomers based on carbon dots, Anal. Chem. 95 (39) (2023) 14573–14581, https://doi.org/10.1021/acs.analchem.3c01854.

[9] J. Gao, X. Chen, S. Chen, H. Meng, Y. Wang, C. Li, L. Feng, The bodipy-based chemosensor for fluorometric/colorimetric dual channel detection of RDX and PA, Anal. Chem. 91 (21) (2019) 13675–13680, https://doi.org/10.1021/acs.analchem.9b02888.

[10] A. Qileng, W. Liu, H. Liang, M. Chen, H. Shen, S. Chen, Y. Liu, Tuning the electronic configuration of oxygen atom in engineering non-self-limited nanozyme for portable immunosensor, Adv. Funct. Mater. 34 (10) (2024), https://doi.org/10.1002/adfm.202311783.
[11] N. Alizadeh, A. Salimi, Multienzymes activity of metals and metal oxide nanomaterials: Applications from biotechnology to medicine and environmental engineering, J. Nanobiotechnol. 19 (1) (2021), https://doi.org/10.1186/s12951-021-00771-1.
[12] K. Boriachek, M.K. Masud, C. Palma, P. Hoang-Phuong, Y. Yamauchi, M.S. A. Hossain, N. Nam-Trung, C. Salomon, M.J.A. Shiddiky, Avoiding pre-isolation step in exosome analysis: Direct isolation and sensitive detection of exosomes using gold-loaded nanoporous ferric oxide nanozymes, Anal. Chem. 91 (6) (2019) 3827–3834, https://doi.org/10.1021/acs.analchem.8b03619.
[13] Z.-M. Li, X.-L. Zhong, S.-H. Wen, L. Zhang, R.-P. Liang, J.-D. Qiu, Colorimetric detection of methyltransferase activity based on the enhancement of coooh nanozyme activity by ssDNA, Sens. Actuators , B 281 (2019) 1073–1079, https://doi.org/10.1016/j.snb.2018.11.085.
[14] J. Liu, Y. Zhu, Y. Fan, L. Gong, X. Zhu, Y. Zhang, M. Liu, S. Yao, The pH-dependent multiple nanozyme activities of copper-cerium dioxide and its application in regulating intracellular oxygen and hydrogen peroxide levels, J. Colloid Interf. Sci. 654 (2024) 1054–1062, https://doi.org/10.1016/j.jcis.2023.10.050.
[15] Y. Xu, P. Li, X. Hu, H. Chen, Y. Tang, Y. Zhu, X. Zhu, Y. Zhang, M. Liu, S. Yao, Polyoxometalate nanostructures decorated with CuO nanoparticles for sensing ascorbic acid and Fe^{2+} ions, ACS Appl. Nano Mater. 4 (8) (2021) 8302–8313, https://doi.org/10.1021/acsanm.1c01495.
[16] J. Chang, X. Wang, J. Wang, H. Li, F. Li, Nucleic acid-functionalized Metal-Organic Framework-based homogeneous electrochemical biosensor for simultaneous detection of multiple tumor biomarkers, Anal. Chem. 91 (5) (2019) 3604–3610, https://doi.org/10.1021/acs.analchem.8b05599.
[17] B. Fang, X. Liu, J. Peng, Y. Li, Z. Gong, W. Lai, Dramatic fluorescence enhancement of PCN-224 and its application in "turn off" immunoassay for sensitive detection of e. Coli o157:H7 in milk, 138749-138749, Food Chem. 445 (2024), https://doi.org/10.1016/j.foodchem.2024.138749.
[18] G. Xing, Y. Shang, J. Ai, H. Lin, Z. Wu, Q. Zhang, J.-M. Lin, Q. Pu, L. Lin, Nanozyme-mediated catalytic signal amplification for microfluidic biosensing of foodborne bacteria, Anal. Chem. 95 (35) (2023) 13391–13399, https://doi.org/10.1021/acs.analchem.3c03232.
[19] L. Ren, F. Hong, L. Zeng, Y. Chen, Three-in-one" Zr-MOF multifunctional carrier-mediated fluorescent and colorimetric dual-signal readout biosensing platform to enhance analytical performance, ACS Appl. Mater. Interfaces 14 (45) (2022) 51234–51243, https://doi.org/10.1021/acsami.2c16267.
[20] Z. Wang, B. Liu, Q. Sun, S. Dong, Y. Kuang, Y. Dong, F. He, S. Gai, P. Yang, Fusiform-like copper(ii)-based Metal-Organic Framework through relief hypoxia and gsh-depletion co-enhanced starvation and chemodynamic synergetic cancer therapy, ACS Appl. Mater. Interfaces 12 (15) (2020) 17254–17267, https://doi.org/10.1021/acsami.0c01539.
[21] Y. Ma, F. Li, X. Ren, W. Chen, C. Li, P. Tao, C. Song, W. Shang, R. Huang, B. Lv, H. Zhu, T. Deng, J. Wu, Facets matching of platinum and ferric oxide in highly efficient catalyst design for low-temperature co oxidation, ACS Appl. Mater. Interfaces 10 (17) (2018) 15322–15327, https://doi.org/10.1021/acsami.8b03579.
[22] J. Wang, X. Shao, Q. Zhang, G. Tian, X. Ji, W. Bao, Preparation of mesoporous magnetic Fe_2O_3 nanoparticle and its application for organic dyes removal, J. Mol. Liq. 248 (2017) 13–18, https://doi.org/10.1016/j.molliq.2017.10.026.
[23] J. Wang, Y. Fan, Y. Tan, X. Zhao, Y. Zhang, C. Cheng, M. Yang, Porphyrinic metal-organic framework PCN-224 nanoparticles for near-infrared-induced attenuation of aggregation and neurotoxicity of alzheimer's amyloid-β peptide, ACS Appl. Mater. Interfaces 10 (43) (2018) 36615–36621, https://doi.org/10.1021/acsami.8b15452.
[24] W. Dong, Z. Li, W. Wen, B. Liu, G. Wen, Novel CdS/MOF cathodic photoelectrochemical (PEC) platform for the detection of doxorubicin hydrochloride and gentamicin sulfate, ACS Appl. Mater. Interfaces 13 (48) (2021) 57497–57504, https://doi.org/10.1021/acsami.1c19481.
[25] L. Minati, V. Micheli, B. Rossi, C. Migliaresi, L. Dalbosco, G. Bao, S. Hou, G. Speranza, Application of factor analysis to XPS valence band of superparamagnetic iron oxide nanoparticles, Appl. Surf. Sci. 257 (24) (2011) 10863–10868, https://doi.org/10.1016/j.apsusc.2011.07.123.
[26] Z. Luo, W. Xu, Z. Wu, L. Jiao, X. Luo, M. Xi, R. Su, L. Hu, W. Gu, C. Zhu, Iron single-atom catalyst-enabled peroxydisulfate activation enhances cathodic electrochemiluminescence of tris(bipyridine)ruthenium(ii), Anal. Chem. 95 (28) (2023) 10762–10768, https://doi.org/10.1021/acs.analchem.3c01822.
[27] L. Yang, N. Jiang, Z. Zhang, X. Zhang, H. Wu, Z. Li, Z. Zhou, A Zn-modified PCN-224 fluorescent nanoprobe for selective and sensitive turn-on detection of glutathione, Talanta 270 (2024), https://doi.org/10.1016/j.talanta.2024.125652.
[28] J. Ma, W. Wang, Y. Li, Z. Lu, X. Tan, H. Han, Novel porphyrin Zr Metal-Organic Framework (PCN-224)-based ultrastable electrochemiluminescence system for pedv sensing, Anal. Chem. 93 (4) (2021) 2090–2096, https://doi.org/10.1021/acs.analchem.0c03836.
[29] Z. Guan, S. Zhu, S. Ding, D. Xia, D. Li, Fe-O-Zr in MOF for effective photo-fenton bisphenol a degradation: Boosting mechanism of electronic transmission, Chemosphere 299 (2022), https://doi.org/10.1016/j.chemosphere.2022.134481.
[30] J. Guo, S. Wu, Y. Wang, M. Zhao, A label-free fluorescence biosensor based on a bifunctional MiL-101(Fe) nanozyme for sensitive detection of choline and acetylcholine at nanomolar level, Sens. Actuators, B 312 (2020), https://doi.org/10.1016/j.snb.2020.128021.
[31] K. Yu, T. Wei, Z. Li, J. Li, Z. Wang, Z. Dai, Construction of molecular sensing and logic systems based on site-occupying effect-modulated MOF-DNA interaction, J. Am. Chem. Soc. 142 (51) (2020) 21267–21271, https://doi.org/10.1021/jacs.0c10442.
[32] J. Chen, H. Zhang, U. Farooq, Q. Zhang, J. Ni, R. Miao, W. Chen, Z. Qi, Transport of dissolved organic matters derived from biomass-pyrogenic smoke (sdoms) and their effects on mobility of heavy metal ions in saturated porous media, 139247-139247, Chemosphere 336 (2023), https://doi.org/10.1016/j.chemosphere.2023.139247.
[33] H. Feng, S. Ma, Z. Chen, Y. Li, M. Wang, Y. Ding, Adsorption of nucleotides and nucleic acids on goethite nanoparticles: Mode, sites and relationship with phosphate and non-phosphate structures, Environ. Sci. -Nano (2024) 2655–2667, https://doi.org/10.1039/d3en00891f.
[34] F. Li, X. Hu, F. Wang, B. Zheng, J. Du, D. Xiao, A fluorescent "on-off-on" probe for sensitive detection of ATP based on ATP displacing DNA from nanoceria, Talanta 179 (2018) 285–291, https://doi.org/10.1016/j.talanta.2017.09.091.
[35] S.-X. Lin, W.-L. Pan, R.-J. Niu, Y. Liu, J.-X. Chen, W.-H. Zhang, J.-P. Lang, D. J. Young, Effective loading of cisplatin into a nanoscale UiO-66 Metal-Organic Framework with preformed defects, Dalton T 48 (16) (2019) 5308–5314, https://doi.org/10.1039/c9dt00719a.
[36] S.K. Gupta, S.P. Tripathy, D. Bharti, S.K. Pal, S. Verma, K. Pal, S.S. Ray, One pot synthesis of phosphate glass with in situ formed nanodiamonds from adenosine triphosphate for bone repair, Ceram. Int. 49 (13) (2023) 22537–22546, https://doi.org/10.1016/j.ceramint.2023.04.089.
[37] Z. Yao, B. Huang, X. Hu, L. Zhang, D. Li, M. Guo, X. Zhang, H. Yuan, H.-C. Wu, Colorimetric detection of copper ions based on a supramolecular complex of water-soluble polythiophene and ATP, Analyst 138 (6) (2013) 1649–1652, https://doi.org/10.1039/c3an00151b.
[38] L. Song, J. Nan, B. Liu, F. Wu, Novel three-dimensional Ti_3C_2-Mxene embedded zirconium alginate aerogel adsorbent for efficient phosphate removal in water, Chemosphere 319 (2023), https://doi.org/10.1016/j.chemosphere.2023.138016.
[39] W. Zhou, Z. Hu, J. Wei, H. Lu, H. Dai, J. Zhao, W. Zhang, R. Guo, A ratiometric fluorescent probe based on PCN-224 for rapid and ultrasensitive detection of copper ions, Compos. Commun. 33 (2022), https://doi.org/10.1016/j.coco.2022.101221.

Yani Liu is currently a postgraduate student in Hunan Normal University. Her research mainly focuses on the optical sensors based on nanozymes.

Haoyu Chen is currently a Doctoral student in Hunan Normal University. Her research mainly focuses on optical sensors and nanocatalysis in therapy.

Lin Chai is currently an undergraduate student in Hunan Normal University. Her research mainly focuses on nanomaterials.

Jing Liu is currently a Doctoral student in Hunan Normal University. Her research mainly focuses on the novel nanomaterials in biosensing and therapy.

Shu Huang is an associate chief physician in the Department of Orthopedics at Hunan Provincial People's Hospital, Hunan Normal University.

Feng Liu received his PhD degree in Hunan University in 2020. He joined in Hunan Normal University in 2023. His research mainly focuses on design and synthesis of organic small molecule probes.

Mingjie Wei received his PhD degree in Zhongshan University. He joined in Hubei University of Science and Technology in 2020. His research mainly focuses on fluorescence probes and biosensing.

Xiaohua Zhu received his PhD degree in Hunan University in 2020. He joined in Hunan Normal University in 2023. His research mainly focuses on design and synthesis of organic small molecule probes.

Youyu Zhang received her PhD degree in Hunan University in 2004. She is a professor in Hunan Normal University since 2005. Her research mainly focuses on nanomaterials preparation and application.

Meiling Liu received her PhD degree in Hunan Normal University in 2012. She is a professor in Hunan Normal University since 2018. During 2017–2018, she worked as a visiting scholar at University of California, Los Angeles. Her research mainly focuses on electrochemical sensing and electrocatalysis.

Shouzhuo Yao is an academician of the Chinese Academy of Science.